Trajectory and Attitude Control for a Lunar lander Using a Reference Model (2nd Report)

Akio Abe, Kenji Uchiyama and Yuzo Shimada
Department of Aerospace Engineering College of Science and Technology, Nihon University
7-24-1 Narashinodai, Funabashi, Chiba 274-8501, Japan
(Tel: +81-47-469-5390 ; Fax: +81-47-467-9569 ; E-mail: abeaero@hotmail.com)

ABSTRACT: In this paper, a redesigned guidance and control system for a lunar lander is presented. In past studies, the authors developed a trajectory and attitude control system which achieves the vertical soft landing on the lunar surface. It is confirmed that the system has a good tracking ability to a predefined profile and good robustness against a thruster failure mode where a partial failure of clustered engines was assumed. However, under the previous control laws, the landing point tends to be shifted, in response to the system parameter values, from a target point. Also, an unbalanced moment due to a thruster failure mode was not considered in the simulation. Therefore, in this study, the downrange control is added to the system to enable the vehicle to land at a pre-assigned target point accurately. Furthermore, inhibiting the effect of the unbalanced moment is attempted thorough redesigning the attitude control system. A numerical simulation was performed to confirm the ability of the proposed system with regard to the above problems. Moreover, in the past simulations, a low initial altitude was assumed as an initial condition: in this study, however, the performance of the proposed system is examined over the whole trajectory from an initial altitude of 10 [km] to the lunar surface.

Keywords: Nonlinear control, Lunar lander, Vertical soft landing, Gravity-turn, Lyapunov direct method

1. INTRODUCTION

To date, guidance and control (GC) systems for a lunar lander have been widely studied. In the GC system, an accurate vertical soft landing at the target point and robustness against disturbances such as thrust failure are required.

Table 1 shows the results of past and present studies (Ref. [1]～[5]). Throughout these studies, a gravity-turn descent is assumed in order to achieve the vertical landing.

Originally, this study was initiated by McInnes of the University of Glasgow in the United Kingdom in 1998. He derived the direct adaptive control law which tracks the vehicle to a predefined velocity-altitude profile, which provides a semiminimal fuel consumption trajectory for the gravity-turn decent (Ref. [1]). Also, his method provides the lander with a compensation mechanism against the partial failure mode of clustered thrusters.

In 2000, Shimada, one of the present authors, revealed that McInnes' control law was not sufficient for stability, and he developed the nonlinear robust trajectory control law which introduced a concept of ideal error dynamics in order to improve the speed of error convergence. This control law possesses a better convergence property of the velocity error and has greater robustness against the thruster failure mode than McInnes' method (Ref. [2]).

In 2002, the authors added altitude control to the GC system since in the previous two methods, only the velocity could be controlled in spite of using both the altitude and velocity signals (Refs. [3],[4]).

At the ICCAS Conference in autumn 2002, the authors presented for the first time, the attitude control portion added to the GC system to guarantee the gravity-turn descent (Ref.[5]). However, under these control laws adopted, the landing point was apt to deviate from the target point since the downrange was not controlled.

Furthermore, to date, the authors have not taken into account the effect of the unbalanced moment caused by thruster failure. In addition, a low initial altitude has been chosen in accordance with McInnes (Ref.[1]) in order to compare our method with his method.

Therefore, in this study, the authors attempt to design a trajectory and attitude control system which satisfies an accurate touch down position and inhibits the effect of the unbalanced moment.

Numerical simulation is performed to confirm the tracking ability of the state variables to the reference states, and the ability to deal with the lack of the thruster and the effect of its unbalanced moment. Furthermore, in the simulation, the initial altitude is extended to a higher altitude, a circular orbit of 10 [km], in order to examine the performance of the proposed system.

Table 1 Performance evaluations of control systems.

		Position Control		Velocity	Vertical	Soft	Attitude
		Downrange	Altitude	Control	Landing	Landing	Control
1998	McInnes	--	--	△	○	○	--
2000	Our Study	--	--	○	○	○	--
2002	Our Study	--	○	○	○	○	--
2002	Our Study	--	○	○	○	○	△
2003	Present Study	○	○	○	○	○	○

○： good ，△： satisfied， -- nothing

2. DYNAMICS OF LUNAR LANDER

Figure 1 illustrates the descent motion of the lunar lander. In the figure, ***v***, ***T*** and ***mg*** denote the velocity, thrust and gravity vectors, respectively. In the formulation of the lunar landing model, the translational and rotational motions are taken into account and the flat surface model is assumed. The rotation of the moon is not considered.

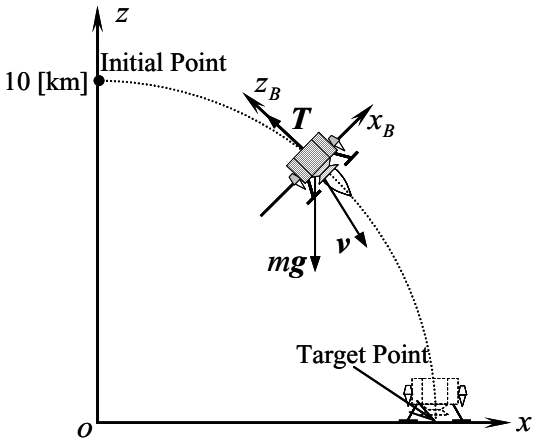

Fig.1 Descent Motion of the Lunar Lander

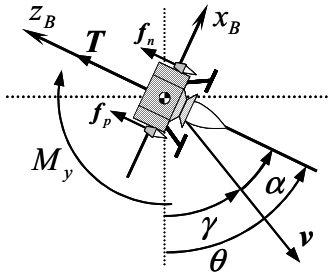

Fig.2 Notations

The local vertical-horizontal coordinates, *o-xz*, fixed on the lunar surface are regarded as an inertial coordinate system. Figure 2 shows definitions of the flight path angle γ, the attitude angle θ, the angle of attack α, and the pitching moment *M*. These angles must satisfy the following relationship.

$$\theta(t) = \gamma(t) + \alpha(t) \tag{1}$$

As shown in Figure 2, in the gravity-turn descent, the direction of the thrust vector must be controlled in order to be opposite to that of the velocity vector. For this purpose, side thrusters are used to produce the pitching moment M_y.

The motion of the lunar lander can be described in the following nonlinear form.

$$\dot{\boldsymbol{x}}(t) = \boldsymbol{f}(\boldsymbol{x},t) + \boldsymbol{g}(\boldsymbol{x},t)\boldsymbol{u}(t) + \boldsymbol{d}(t) \tag{2}$$

$$\boldsymbol{f}(\boldsymbol{x},t) = \begin{bmatrix} -v\sin\alpha + \dot{\theta} z_B \\ -v\cos\alpha - \dot{\theta} x_B \\ g\cos\gamma(t) \\ -(g/v)\sin\gamma \\ q(t) \\ 0 \end{bmatrix}, \quad \boldsymbol{g}(\boldsymbol{x},t) = \begin{bmatrix} 0 & 0 \\ 0 & 0 \\ -g\cos\alpha & 0 \\ (g/v)\sin\alpha & 0 \\ 0 & 0 \\ 0 & 1/I_{yy} \end{bmatrix}$$

$$\boldsymbol{x}(t) = [x_B(t),\, z_B(t),\, v(t),\, \gamma(t),\, q(t)]^T$$
$$\boldsymbol{u}(t) = [n(t),\, M_y(t)]^T$$
$$\boldsymbol{d}(t) = [0,\, 0,\, 0,\, 0,\, M_{yD}/I_{yy}]^T$$

Here, x_B and z_B, are the positions, v the velocity, γ the flight path angle, θ the attitude angle, and q the pitch rate. I_{yy} is the moment of inertia of the lander about the y_B axis and M_{yD} is the unbalanced moment caused by the thruster failure mode. The control input $\boldsymbol{u}$ consists of the thrust-to-weight ratio $n=T/mg$ and the pitching moment M_y.

As mentioned before, to perform the gravity-turn descent, the angle of attack α must be maintained as zero in Eq.(1) along the trajectory. Namely, the attitude angle θ must be controlled by the attitude control system, to coincide with the flight path angle γ.

$$\theta(t) = \gamma(t) \quad s.t. \quad \alpha(t) = 0 \tag{3}$$

3. CONTROL SYSTEM DESIGN

3.1 Nominal Motion

In the present study, the nominal gravity-turn descent is regarded as an ideal motion to be followed by the lander. This ideal model (nominal model) can be described by the following equation.

$$\begin{bmatrix} \dot{x}_{Bnom}(t) \\ \dot{z}_{Bnom}(t) \\ \dot{v}_{nom}(z) \end{bmatrix} = \begin{bmatrix} \dot{\gamma}_{nom}(t) z_{Bnom}(t) \\ -v_{nom}(z) - \dot{\gamma}_{nom}(t) x_{Bnom}(t) \\ v_{nom}(z(0))[1 - \exp\{-\lambda z(t)\}] \end{bmatrix} \tag{4}$$

$$\boldsymbol{x}_{Tnom} = [x_{Bnom}(t),\, z_{Bnom}(t),\, z_{Bnom}(t)]^T$$

Here, the nominal velocity v_{nom} in the third row is defined as an exponential function of the actual altitude z according to Ref.[1]. The first and second rows are obtained from Eq.(2) under the conditions of the gravity-turn.

3.2 Actual Error Dynamics

The actual error dynamics is introduced to guarantee the stability of the dynamical system, in Eq.(2). The error in the trajectory control $\boldsymbol{e}_T$ is defined as

$$\begin{bmatrix} e_{x_B}(t) \\ e_{z_B}(t) \\ e_v(t) \end{bmatrix} = \begin{bmatrix} x_B(t) - x_{Bnom}(t) \\ z_B(t) - z_{Bnom}(t) \\ v(t) - v_{nom}(z) \end{bmatrix}$$
$$\Leftrightarrow \quad \boldsymbol{e}_T(t) = \boldsymbol{x}_T(t) - \boldsymbol{x}_{Tnom}(t), \tag{5}$$

where the nominal state $\boldsymbol{x}_{Tnom}$ is a solution of Eq.(4).

Differentiating Eq.(5) and using Eqs.(2) and (4) under the condition of $\alpha(t)$ =0, a linear time-varying (LTV) error model can be obtained:

$$\dot{\boldsymbol{e}}_T(t) = \boldsymbol{A}_T(t)\boldsymbol{e}_T(t) + \boldsymbol{b}_T\, u_1(t) + \boldsymbol{d}_T(t) \tag{6}$$

$$\boldsymbol{A}_T(t)=\begin{bmatrix} 0 & a_{12}(t) & 0 \\ -a_{12}(t) & 0 & -1 \\ 0 & 0 & a_{33}(t) \end{bmatrix}$$

$$\boldsymbol{b}_T=[0,\,0,\,b_3]^T \quad \boldsymbol{d}_T(t)=[0,\,0,\,d_3(t)]^T$$

$$a_{12}(t)=\dot{\theta}(t), \quad a_{33}(t)=(\partial v_{nom}/\partial z)\cos\theta(t)$$

$$b_3(t)=-g\,,\;\; d_3(t)=\{g+(\partial v_{nom}/\partial z)v_{nom}\}\cos\theta(t)\,.$$

In order to obtain a controllable-canonical-like form, a new error vector $\boldsymbol{e}_{T\xi}$ is defined by using a matrix $\boldsymbol{T}_C$.

$$\boldsymbol{e}_{T\xi}(t)=\boldsymbol{T}_C^{-1}(t)\boldsymbol{e}_T(t)=\boldsymbol{T}_C^{-1}(t)\{\boldsymbol{x}_T(t)-\boldsymbol{x}_{Tnom}(t)\} \quad (7)$$

$$\boldsymbol{T}_C(t)=\begin{bmatrix} -a_{12}(t)b_{31} & 0 & 0 \\ 0 & -b_{31} & 0 \\ -a_{12}{}^2(t)b_{31} & 0 & b_{31} \end{bmatrix} \quad (8)$$

Using this transformation, we obtained

$$\dot{\boldsymbol{e}}_{T\xi}(t)=\boldsymbol{A}_C(t)\boldsymbol{e}_{T\xi}(t)+\boldsymbol{b}_C u_1(t)+\boldsymbol{d}_C(t) \quad (9a)$$

$$\boldsymbol{e}_{T\xi}(t)=[\boldsymbol{e}_{\xi_1}(t),\boldsymbol{e}_{\xi_2}(t),\boldsymbol{e}_{\xi_3}(t)]^T$$

$$=[-e_{x_B}/(a_{12}b_{31}),e_{z_B}/b_{31},(a_{12}e_{x_B}+e_v)/b_{31}]^T \quad (9b)$$

$$\boldsymbol{d}_C(t)=\boldsymbol{T}_C^{-1}(t)\boldsymbol{d}_T(t)=[0,\,0,\,d_3(t)/b_3]^T\,. \quad (9c)$$

$$\boldsymbol{A}_C(t)=\boldsymbol{T}_C^{-1}(t)\{\boldsymbol{A}_T(t)\boldsymbol{T}_C(t)-\dot{\boldsymbol{T}}_C(t)\}$$

$$=\begin{bmatrix} -\dot{a}_{12}(t)/a_{12}(t) & 1 & 0 \\ 0 & 0 & 1 \\ a_{12}(t)\{a_{33}(t)-\dot{a}_{12}(t)\} & -a_{12}{}^2(t) & a_{33}(t) \end{bmatrix} \quad (9d)$$

$$\boldsymbol{b}_C=\boldsymbol{T}_C^{-1}(t)\boldsymbol{b}_T=[0,\,0,\,1]^T \quad (9e)$$

Next, we consider the attitude control system. In order to achieve the gravity-turn, another error vector is defined as follows:

$$\begin{bmatrix} e_\theta(t) \\ e_q(t) \end{bmatrix}=\begin{bmatrix} \alpha(t) \\ \dot{\alpha}(t) \end{bmatrix}=\begin{bmatrix} \theta(t)-\gamma(t) \\ \dot{\theta}(t)-\dot{\gamma}(t) \end{bmatrix}$$

$$\Leftrightarrow \quad \boldsymbol{e}_A(t)=\boldsymbol{x}_A(t)-\boldsymbol{x}_{Anom}(t)\,. \quad (10)$$

Differentiating the above equation with respect to time, the following error equation can be obtained.

$$\begin{bmatrix} \dot{e}_\theta(t) \\ \dot{e}_q(t) \end{bmatrix}=\begin{bmatrix} 0 & 1 \\ 0 & a_{55}(t) \end{bmatrix}\begin{bmatrix} e_\theta(t) \\ e_q(t) \end{bmatrix}+\begin{bmatrix} 0 \\ b_{52} \end{bmatrix}u_2(t)+\begin{bmatrix} 0 \\ d_5(t) \end{bmatrix}$$

$$\Leftrightarrow \quad \dot{\boldsymbol{e}}_A(t)=\boldsymbol{A}_A(t)\boldsymbol{e}_A(t)+\boldsymbol{b}_A u_2(t)+\boldsymbol{d}_A(t) \quad (11)$$

$$a_{55}(t)=-\{(n(t)-2\cos\gamma(t))g\}/v(t)\,, \quad b_{52}=1/I_{yy}$$

$$d_5(t)=\{(n(t)-2\cos\gamma(t))gq(t)\}/v(t)$$

Next, combining the vectors $\boldsymbol{e}_{T\xi}$ and $\boldsymbol{e}_A$ into one vector

$$\boldsymbol{e}(t)=\begin{bmatrix} \boldsymbol{e}_{T\xi}(t) \\ \boldsymbol{e}_A(t) \end{bmatrix}=\begin{bmatrix} \boldsymbol{T}_C^{-1}(t)\boldsymbol{e}_T(t) \\ \boldsymbol{e}_A(t) \end{bmatrix}, \quad (12)$$

the whole actual error dynamics can be rewritten as follows:

$$\begin{bmatrix} \dot{\boldsymbol{e}}_{T\xi}(t) \\ \dot{\boldsymbol{e}}_A(t) \end{bmatrix}=\begin{bmatrix} \boldsymbol{A}_C & \boldsymbol{0}_{3\times2} \\ \boldsymbol{0}_{2\times3} & \boldsymbol{A}_A \end{bmatrix}\begin{bmatrix} \boldsymbol{e}_{T\xi}(t) \\ \boldsymbol{e}_A(t) \end{bmatrix}+\begin{bmatrix} \boldsymbol{b}_C & \boldsymbol{0}_{3\times1} \\ \boldsymbol{0}_{2\times1} & \boldsymbol{b}_A \end{bmatrix}\begin{bmatrix} u_1 \\ u_2 \end{bmatrix}+\begin{bmatrix} \boldsymbol{d}_C \\ \boldsymbol{d}_A \end{bmatrix}$$

$$\Leftrightarrow \quad \dot{\boldsymbol{e}}(t)=\boldsymbol{A}(t)\boldsymbol{e}(t)+\boldsymbol{B}\,\boldsymbol{u}(t)+\boldsymbol{d}(t) \quad (13)$$

In order to guarantee stability in the actual error model, the following control law is employed.

$$\boldsymbol{u}(t)=-\boldsymbol{K}(t)\boldsymbol{e}(t)+\boldsymbol{s}(t) \quad (14)$$

$$\boldsymbol{K}(t)=\begin{bmatrix} k_1(t) & k_2(t) & k_3(t) & 0 & 0 \\ 0 & 0 & 0 & k_4(t) & k_5(t) \end{bmatrix}$$

$$\boldsymbol{s}(t)=[s_1(t),\,s_2(t)]^T$$

Here, the matrix $\boldsymbol{K}(t)$ consists of variable gains and its components $k_1(t)$, $k_2(t)$ and $k_4(t)$ affect the natural frequencies of the controlled system. $k_3(t)$ and $k_5(t)$ also affect the damping properties. Here, the vector $\boldsymbol{s}$ designates a new control vector which is defined in section 3.5.

3.3 Ideal Error Dynamics

In this section, ideal error dynamics is introduced so as to improve the convergence property of the actual error dynamics. The ideal error $\boldsymbol{e}_m$ is defined as the difference between the ideal states $\boldsymbol{x}_m$ of a reference model (see Fig.3) and the nominal states $\boldsymbol{x}_{nom}$.

$$\boldsymbol{e}_m(t)=\begin{bmatrix} \boldsymbol{e}_{mT\xi}(t) \\ \boldsymbol{e}_{mA}(t) \end{bmatrix}=\begin{bmatrix} \boldsymbol{T}_C^{-1}(t)\{\boldsymbol{x}_{mT}(t)-\boldsymbol{x}_{nomT}(t)\} \\ \boldsymbol{x}_{mA}(t)-\boldsymbol{x}_{nomA}(t) \end{bmatrix} \quad (15)$$

The ideal error dynamics is defined by the following equation.

$$\begin{bmatrix} \dot{\boldsymbol{e}}_{mT\xi}(t) \\ \dot{\boldsymbol{e}}_{mA}(t) \end{bmatrix}=\begin{bmatrix} \boldsymbol{A}_{mC} & \boldsymbol{0}_{3\times2} \\ \boldsymbol{0}_{2\times3} & \boldsymbol{A}_{mA} \end{bmatrix}\begin{bmatrix} \boldsymbol{e}_{mT\xi}(t) \\ \boldsymbol{e}_{mA}(t) \end{bmatrix}+\begin{bmatrix} \boldsymbol{d}_{mC} \\ \boldsymbol{d}_{mA} \end{bmatrix}$$

$$\Leftrightarrow \quad \dot{\boldsymbol{e}}_m(t)=\boldsymbol{A}_m\boldsymbol{e}_m(t)+\boldsymbol{d}_m \quad (16)$$

$$\boldsymbol{e}_{mT\xi}(t)=[e_{m\xi_1}(t),e_{m\xi_2}(t),e_{m\xi_3}(t)]^T\,,$$

$$\boldsymbol{e}_{mA}(t)=[e_{m\theta}(t),e_{mq}(t)]^T$$

$$\boldsymbol{A}_{mC}=\begin{bmatrix} 0 & 1 & 0 \\ 0 & 0 & 1 \\ -a_{m1} & -a_{m2} & -a_{m3} \end{bmatrix}, \quad \boldsymbol{A}_{mA}=\begin{bmatrix} 0 & 1 \\ -a_{m4} & -a_{m5} \end{bmatrix}$$

$$\boldsymbol{d}_{mC}=[0,\,0,\,d_{m3}]^T\,, \quad \boldsymbol{d}_{mA}=[0,\,d_{m5}]^T$$

Note that the coefficient matrix $\boldsymbol{A}_m$ consists of two controllable canonical forms, which are introduced in order to cancel the three 1s in $\boldsymbol{A}_{\rm m}$ and $\boldsymbol{A}(t)$ in Eq. (19).

3.4 Tracking Error Model

In this section, a third error model is also introduced as below in order to make the actual error track the ideal error,

$$\boldsymbol{\varepsilon}(t)=\boldsymbol{e}_m(t)-\boldsymbol{e}(t)=\begin{bmatrix} \boldsymbol{e}_{mT\xi}(t) \\ \boldsymbol{e}_{mA}(t) \end{bmatrix}-\begin{bmatrix} \boldsymbol{e}_{T\xi}(t) \\ \boldsymbol{e}_A(t) \end{bmatrix}. \quad (17)$$

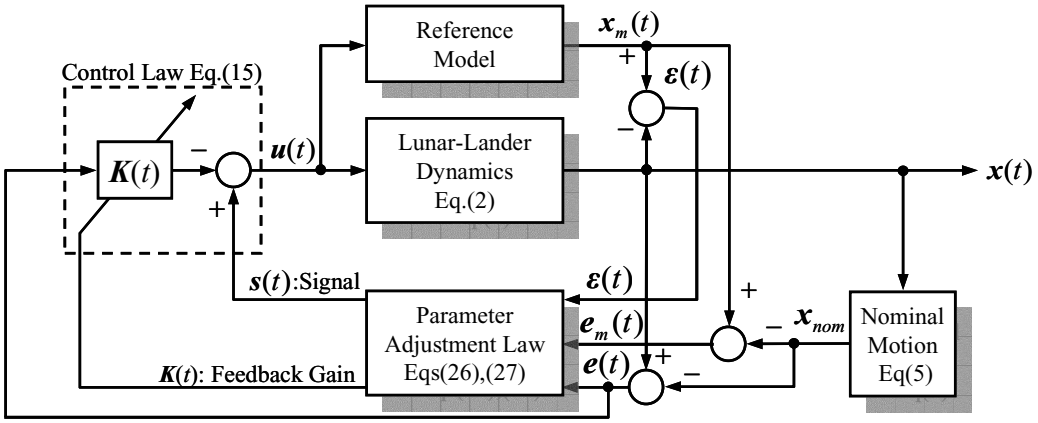

Fig.3 Block diagram of the guidance and control system

Rewriting this equation, the right-hand side becomes the difference between the reference model and the actual lunar lander.

$$\boldsymbol{\varepsilon}(t)=\begin{bmatrix}\boldsymbol{T}_C^{-1}(t)\{\boldsymbol{x}_{mT}(t)-\boldsymbol{x}_T(t)\}\\ \boldsymbol{x}_{mA}(t)-\boldsymbol{x}_A(t)\end{bmatrix} \tag{18}$$

Then, differentiating this equation, the tracking error dynamics is obtained in the following form.

$$\dot{\boldsymbol{\varepsilon}}(t)=\boldsymbol{A}_m\boldsymbol{\varepsilon}(t)+\quad\boldsymbol{A}(t)\boldsymbol{e}(t)+\quad\boldsymbol{d}(t) \tag{19}$$

$$\boldsymbol{A}(t)=\boldsymbol{A}_m-\{\boldsymbol{A}(t)-\boldsymbol{B}\boldsymbol{K}(t)\} \tag{20a}$$

$$\boldsymbol{d}(t)=\boldsymbol{d}_m-\{\boldsymbol{d}(t)+\boldsymbol{B}\boldsymbol{s}(t)\} \tag{20b}$$

3.5 Lyapunov Direct Method

Next, the Lyapunov direct method is utilized in order to guarantee the stability of the above-described tracking system:

$$V(t)=\boldsymbol{\varepsilon}^T(t)\boldsymbol{P}\boldsymbol{\varepsilon}(t)+tr[\quad\boldsymbol{A}(t)\boldsymbol{Q}_1\quad\boldsymbol{A}^T(t)$$
$$+\quad\boldsymbol{d}^T(t)\boldsymbol{Q}_2\quad\boldsymbol{d}(t)\ge 0,\qquad\boldsymbol{P},\boldsymbol{Q}_1,\boldsymbol{Q}_2\ge 0. \tag{21}$$

Here, the matrices $\boldsymbol{Q}_1$ and $\boldsymbol{Q}_2$ are chosen as the diagonal matrices. Taking the time derivative of the V function, we obtain

$$\dot{V}(t)=\boldsymbol{\varepsilon}^T(t)(\boldsymbol{P}\boldsymbol{A}_m+\boldsymbol{A}_m^T\boldsymbol{P})\boldsymbol{\varepsilon}(t)$$
$$+2tr[\quad\boldsymbol{A}(t)\{\boldsymbol{e}(t)\boldsymbol{\varepsilon}^T(t)\boldsymbol{P}+\boldsymbol{Q}_1\quad\dot{\boldsymbol{A}}^T(t)\}]$$
$$+2\quad\boldsymbol{d}^T(t)\{\boldsymbol{P}\boldsymbol{\varepsilon}(t)+\boldsymbol{Q}_2\quad\dot{\boldsymbol{d}}(t)\}, \tag{22}$$

then, employing

$$\boldsymbol{e}(t)\boldsymbol{\varepsilon}^T(t)\boldsymbol{P}+\boldsymbol{Q}_1\quad\dot{\boldsymbol{A}}^T(t)=-\boldsymbol{R}_1\quad\boldsymbol{A}^T(t) \tag{23}$$

$$\boldsymbol{P}\boldsymbol{\varepsilon}(t)+\boldsymbol{Q}_2\quad\dot{\boldsymbol{d}}(t)=-\boldsymbol{R}_2\quad\boldsymbol{d}(t) \tag{24}$$

$$\boldsymbol{R}_1=\boldsymbol{R}_1^T\ge 0\ \boldsymbol{R}_2=\boldsymbol{R}_2^T\ge 0;$$

the V function becomes negative semi-definite.

$$\dot{V}(t)=\boldsymbol{\varepsilon}^T(t)(\boldsymbol{P}\boldsymbol{A}_m+\boldsymbol{A}_m^T\boldsymbol{P})\boldsymbol{\varepsilon}(t)-2tr[\quad\boldsymbol{A}(t)\boldsymbol{R}_1\quad\boldsymbol{A}^T(t)]$$
$$-2\quad\boldsymbol{d}^T(t)\boldsymbol{R}_2\quad\boldsymbol{d}(t)\le 0 \tag{25a}$$

$$\boldsymbol{P}\boldsymbol{A}_m+\boldsymbol{A}_m^T\boldsymbol{P}\le 0 \tag{25b}$$

Table 2 Initial conditions and parameters

Initial Conditions					
State Variables	Downrange[m] $x(0)$=0		Altitude[m] $z(0)$=10000		Path Angle [deg] $\gamma(0)=90$
	Velocity [m/s] $v(0)$=100		Attitude Angle [deg] $\theta(0)$=90		Pitch Rate [deg/s] $q(0)$=-0.934
Gains	$k_1(0)$=8	$k_2(0)$=8	$k_3(0)$=4	$k_4(0)$=7615	$k_5(0)$=1795
Signals	$s_1(0)$=0	$s_2(0)$=0			
Parameter set value					
Ideal Error Dynamics	a_{m1}=8	a_{m2}=4	a_{m3}=4	a_{m4}=36	a_{m5}=8.49
	d_{m3}=0	d_{m5}=0			
Adjustment Law	$\boldsymbol{P}=\begin{bmatrix}0&0&p_{13}&0&0\\0&0&p_{23}&0&0\\p_{13}&p_{23}&p_{33}&0&0\\0&0&0&0&p_{45}\\0&0&0&p_{45}&p_{55}\end{bmatrix}=\begin{bmatrix}0&0&500&0&0\\0&0&500&0&0\\500&500&500&0&0\\0&0&0&0&3000000\\0&0&0&3000000&3000000\end{bmatrix}$				
	$\boldsymbol{Q}_1=\boldsymbol{I}_{5\times5},\ \boldsymbol{Q}_2=\boldsymbol{I}_{5\times5}$				
	$\boldsymbol{R}_1=diag[r_{11}\ \ r_{12}\ \ r_{13}\ \ r_{14}\ \ r_{15}]=diag[100\ \ 100\ \ 100\ \ 100000\ \ 100000]$				
	$\boldsymbol{R}_2=diag[r_{21}\ \ r_{22}\ \ r_{23}\ \ r_{24}\ \ r_{25}]=diag[0\ \ 0\ \ 100\ \ 0\ \ 100000]$				

From Eqs.(23) and (24), two laws for the gain adjustment and feedback signal generation are given as the form of the following differential equations:

$$\dot{\boldsymbol{K}}(t) = -(\boldsymbol{B}^T\boldsymbol{B})^{-1}\boldsymbol{B}^T[\{\boldsymbol{P}\boldsymbol{\varepsilon}(t)\boldsymbol{e}^T(t) + \boldsymbol{A}(t)\boldsymbol{R}_1\}\boldsymbol{Q}_1^{-1} + \dot{\boldsymbol{A}}(t)] \quad (26)$$

$$\dot{\boldsymbol{s}}(t) = (\boldsymbol{B}^T\boldsymbol{B})^{-1}\boldsymbol{B}^T[\boldsymbol{Q}_2^{-1}\{\boldsymbol{P}\boldsymbol{\varepsilon}(t) + \boldsymbol{R}_2\ \boldsymbol{d}(t)\} - \dot{\boldsymbol{d}}(t)] \quad (27)$$

Figure 3 shows the block diagram of the proposed guidance and control system.

4. NUMERICAL SIMULATIONS

Numerical simulation was performed to verify the validity of the proposed system. The initial altitude was changed from the altitude of 100 [m] used in Refs 1-5 to 10 [km]. The robustness against the partial thruster failure mode is also investigated. Table 2 shows the initial conditions and the parameter set used in the numerical simulation.

4.1 Results of simulation without thrust failure

Figure 5 shows the trajectory of the lunar lander. The actual trajectory coincides with the nominal (predefined) trajectory. Thus, it was confirmed that the proposed system had a good tracking ability. A minimal downrange error was also achieved compared with those of the previous studies.

The altitude-velocity profile is indicated in Figure 6. As is evident in the figure, soft landing is also achieved. Here, the nominal velocity-altitude profile is calculated from the third row of Eq.(5).

Figures 7 and 8 present the time histories of the control inputs u_1 (thrust-to-weight ratio) and u_2 (pitching moment). Figures 9 and 10 show the time histories of the related angles and their rates. It is clear from these figures that the attitude angle and its rate are correctly controlled so as to coincide with the corresponding variables. That is, since the angle of attack and its rate remain zero, the gravity-turn descent is completed.

4.2 Results of simulation with thrust failure

Next, a thruster failure mode is simulated. As shown in Figure 4, one of the four clustered thrusters was assumed to break down at approximately 150[s] so as to allow only the longitudinal motion; finally, the actual thruster value decreases to 3/4 of the commanded value. Furthermore, an unbalanced moment due to the thruster failure is taken into account in the simulation in order to examine the validity of the attitude control law.

The thruster failure mode is modeled by the following equations.

$$u(t) = f(t)u_{com}(t) \quad (28a)$$

$$f(t) = 0.875 - (0.95/12)\tan^{-1}(t-150) \quad (28b)$$

Figure 11 shows the time histories of the actual and commanded thrust-to-weight ratios. The system automatically regulates u_{com} against the thruster failure mode, in order to maintain u at the same level as that in Figure 7.

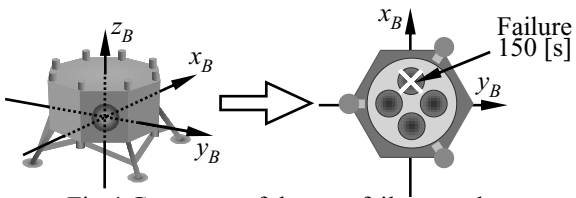

Fig.4 Geometry of thruster failure mode

Figure 12 shows the time history of the pitching moment with the thruster failure mode. The attitude control system generates a countermoment against the unbalanced moment. Thus, the lander maintains a suitable attitude under the proposed attitude control law.

5. CONCLUSION

In this paper, a new trajectory and attitude control system for the lunar lander was presented. The simulation results revealed that the proposed system had a good convergence property and that a vertical soft landing was achieved accurately. It was also confirmed that the proposed control system could compensate for or overcome the lack of thrust and the unbalanced moment due to thruster failure.

ACKNOWLEDGEMENT

This research is supported by a Grant-in Aid for Scientific Research (c). No.14550856, from the Japan Society for the Promotion of Science.

REFERENCE

[1] Colin R. McInnes: Direct Adaptive Control for Gravity Turn Descent, Journal of Guidance, Control and Dynamics *AIAA*, 1998, pp.373-375.

[2] Yuzo Shimada: Nonlinear Robust Trajectory Control Law for a Lunar lander Gravity-Turn Descent, 22nd International Symposium on Space Technology and Science, Morioka, Japan, 2000.

[3] Akio Abe, Kenji Uchiyama and Yuzo Shimada: "Optimal Guidance and Nonlinear Tracking Control for a Lunar lander", Proceedings of the Annual Meeting and the Third Symposium on Propulsion System for Reusable Launch Vehicles, Northern Section of the JSASS, 2002, in Japanese.

[4] Akio Abe, Kenji Uchiyama and Yuzo Shimada: Nonlinear Tracking Control Law for a Lunar Lander, 3rd Pacific Asia Conference of Mechanical Engineering, Philippines, Manila, 2002.

[5] Akio Abe, Kenji Uchiyama and Yuzo Shimada: Trajectory and Attitude Control for a Lunar lander Using a Reference Model, International Conference of Control, Automation and Systems, Muju, Korea, pp.453-458, 2002.

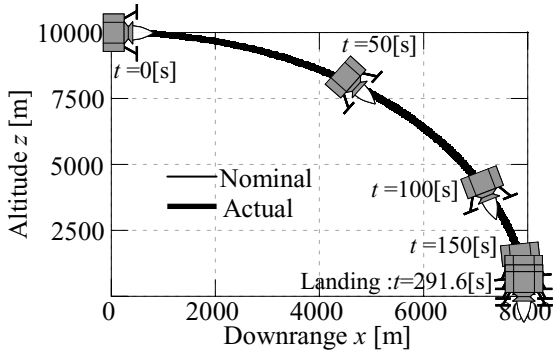

Fig.5 Vehicle trajectory

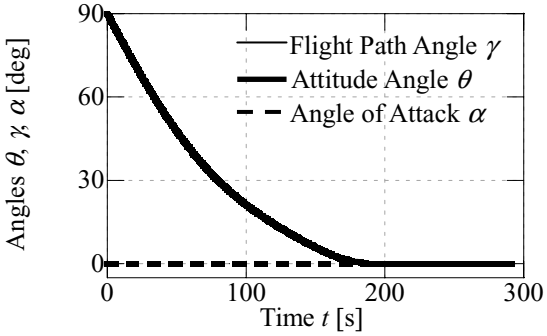

Fig.9 Time histories of angles θ, γ, α

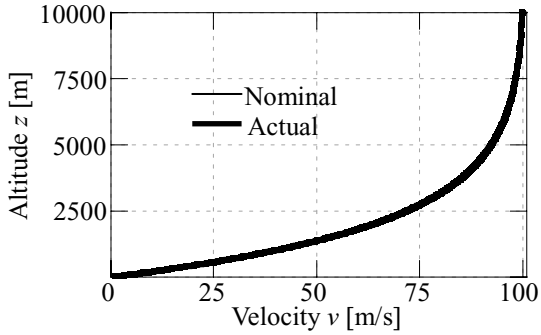

Fig.6 Flight region (Altitude vs Velocity)

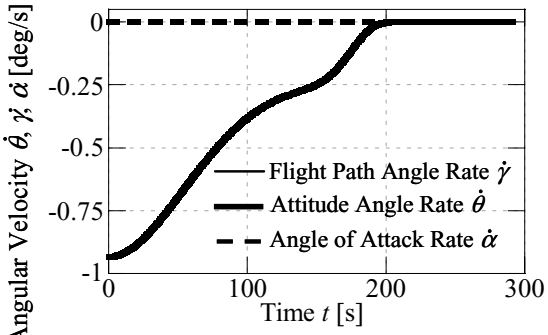

Fig.10 Time histories of angular velocity

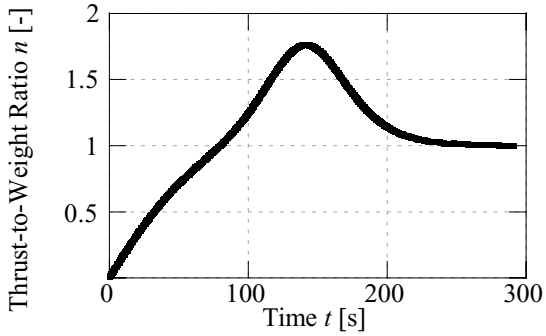

Fig.7 Time history of thrust-to-weight ratio

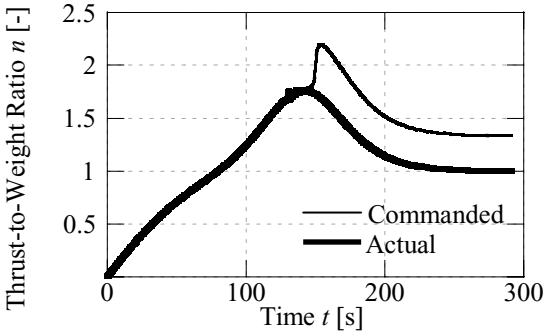

Fig.11 Time histories of actual and commanded thrust-to-weight ratios with thruster failure

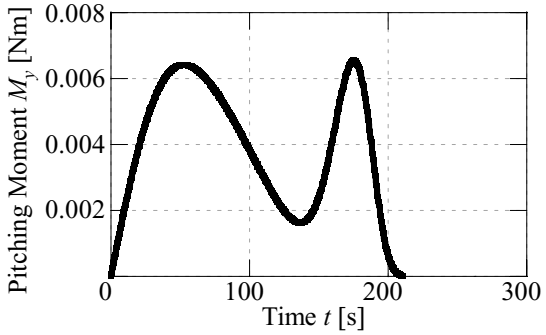

Fig.8 Time history of pitching moment

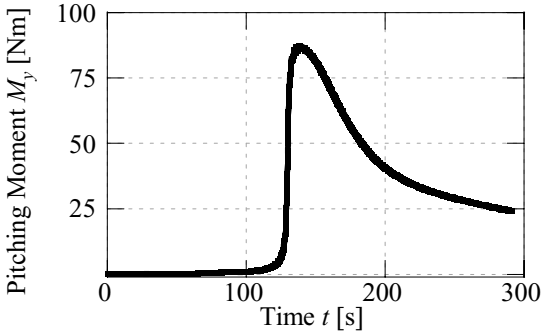

Fig.12 Time history of pitching moment with thruster failure